Laser and Particle Beams

cambridge.org/lpb

Magnetic field effect on plasma parameters and surface modification of laser-irradiated Cu-alloy

Asadullah Dawood, Shazia Bashir, Naveed Ahmed Chishti, Muhammad Asad Khan and Asma Hayat

Centre for Advanced Studies in Physics, Government College University, Lahore, Pakistan

Research Article

Cite this article: Dawood A, Bashir S, Chishti NA, Khan MA, Hayat A (2018). Magnetic field effect on plasma parameters and surface modification of laser-irradiated Cu-alloy. *Laser and Particle Beams* **36**, 261–275. https://doi.org/10.1017/S0263034618000137

Received: 10 January 2018
Accepted: 3 April 2018

Key words:
Cu-alloy; electron density; excitation temperature; LIBS; surface modification

Author for correspondence:
Shazia Bashir, Centre for Advanced Studies in Physics, Government College University, Lahore, Pakistan. E-mail: shaziabashir@gcu.edu.pk

Abstract

The effect of magnetic field on the plasma parameters and surface modification of Cu-alloy has been investigated. For this purpose, we have employed Nd: YAG laser at various irradiances ranging from 1.9 to 5 GW/cm^2 to irradiate Cu-alloy under 5 torr pressure of argon, neon, and helium. The evaluated values of excitation temperature (T_{exc}) and electron number density (n_e) of Cu-alloy plasma explored by laser-induced breakdown spectroscopy technique are higher in the presence of 1.1 Tesla magnetic field as compared with field-free case. It is true at all irradiances as well as under all environmental conditions. It is also found that trends of both T_{exc} and n_e are increasing with increasing laser irradiance from 1.9 to 4.4 GW/cm^2. For the highest used irradiance 5 GW/cm^2, the decrease in both parameters is observed. The analytically calculated values of thermal beta, directional beta, confinement radius, and diffusion time for laser-irradiated Cu-alloy plasma confirm the validity of magnetic confinement. Scanning electron microscope analysis is utilized to study the surface modifications of laser-irradiated Cu samples and reveals the formation of islands, craters, cones, and droplets. The finer-scale surface structures are grown in case of magnetic. It is also revealed T_{exc} and n_e play a substantial part in the growth of surface structures on Cu-alloy.

Introduction

Laser ablation is an emerging technique for material processing due to a wide range of applications in the field of pulsed-laser deposition of thin film, micro/nano-structuring, and machining of materials, plasma processing, and ion-implantation (Amin *et al.*, 2017). Laser-induced breakdown spectroscopy is a promising technique for elemental analysis as well as for evaluating of T_{exc} and n_e of the generated plasma. The employment of the magnetic field of appropriate strength on a laser-induced plasma (LIP) can restrict the free expansion of plasma species and causes various physical processes, for example, magnetic and spatial effects (Neogi and Thareja, 1999) Joule heating effects (Shen *et al.*, 2006) conversion of kinetic energy into plasma thermal energy (Pandey and Thareja, 2011) employment of Lorentz force to provide particular trajectories to charged species (Bashir *et al.*, 2012), and the variation in plasma instabilities (Amin *et al.*, 2017). All these phenomena are responsible for enhancing the T_{exc} and n_e of plasmas. The employment of the magnetic field on plasmas has vast ranging applications in the field of auroral pluses (Raju *et al.*, 2014), deposition of thin films (Joshi *et al.*, 2010), space vehicles propulsion (Kim *et al.*, 2007), development of solar wind (Gekelman *et al.*, 2003), magnetic resonance tomography (Neogi and Thareja, 1999), astrophysical jets (Ott and Manheimer,1977), and magneto hydrodynamic (MHD) generators (Ducruet *et al.*, 2006), etc. In the recent years, application of magnetic field on laser-produced plasma (LPP) has emerged as a promising tool for enhancement of emission intensity, T_{exc}, ion acceleration, and n_e of electrons (Amin *et al.*, 2017; Singh and Sharma, 2017).

Ye *et al.* (2013) revealed that if the magnetic field is applied to Cu films plasma, then enhancement in ablation depth is observed during laser drilling. They also explored that aspect ratio, as well as ns-laser ablation speed can be enriched by applying a constant magnetic field to LPP which is attributed to magnetic confinement of plasma. Pandey *et al.* (2015) explored that LPP dynamics and optical emission intensity of Cu are modified in the presence as well as the absence of magnetic field due to large-scale ablation. Amin *et al.* (2017) investigated that enhancement in optical emission intensity from the magnetically confined plasma of V_2O_5 is observed. As a result increase in T_{exc} and n_e is observed. Shen *et al.* (2006) explored the effect of the presence of magnetic field on emission intensity in atomic as well as in ionic transitions of Cu. Their study revealed that enhancement in both types of emissions was observed. Rai *et al.* (2003) studied the effect of magnetic field on LPP of solid as well as liquid samples. They revealed that the enhancement in emission intensity strongly relies on physical properties of a specimen. Their study also depicted that by increasing fluence an increase in emission

CAMBRIDGE UNIVERSITY PRESS

intensity is observed and afterward it showed a saturation. Raju *et al.* (2014) reviewed the expansion dynamics and spectral behavior of the barium plasma produced by an Nd:YAG laser in the presence of the 0.45T transverse magnetic field in a vacuum using time-of-flight optical emission spectroscopy at various laser fluences.

Cu is widely investigated metal for plasma generation as well as laser ablation due to high electrical conductivity, high ductility. Laser-produced copper plasma is also used to synthesize nanoparticles for application in solar cells, sensors, LED, catalyst, antifungal, and bacterial activities (Singh and Sharma, 2017). Cu alloy (Gilding metal) is utilized for different purposes, including the coats of slugs, driving groups on some cannons shells and in addition enameled identifications and other gems. The sheet is generally utilized to create metalworking by pound work. It is additionally utilized especially as a lower-cost preparing material for silversmiths (WikiPedia). Pure Cu metal is widely investigated for laser-induced breakdown spectroscopy (LIBS) as well as laser-induced structuring but a scarce work is represented on Cu-alloy which is highly useful material for industrial applications.

In the present work, the effect of magnetic field on laser-ablated Cu-alloy plasma parameters along with surface structuring is explored and their correlation is being established. The assembly of two permanent magnets is used to generate a transverse magnetic field of strength 1.1 Tesla. LIBS technique is employed to explore LPP of Cu under different ambient environments of Ar, Ne, and He at different irradiances ranging from 1.9 to 5 GW/cm^2 at a fixed optimized pressure of 5 Torr. Cu plasma is characterized by two plasma parameters, that is T_{exc} and n_e. T_{exc} is explored by the Boltzmann plot method whereas n_e is explored by using Stark broadening method. After irradiation surface structures are grown which are explored by scanning electron microscope (SEM) analysis. We have analytically calculated the plasma confinement parameters like thermal β_t-parameter, directed beta β_d, confinement radius (R_b) and diffusion time t_d of Cu plasma in all ambient environments at various irradiances. These parameters are important for confirming the validity of magnetic confinement in the presence of 1.1 Tesla magnetic field.

Experimental setup

Figure 1 depicts the schematic of the experimental setup. Experiments were performed by employing Nd: YAG laser (1.06 μm) with laser irradiance ranging from 1.9–5 GW/cm^2, at a pulse duration of 10 ns and at a repetition rate of 1–10 Hz. Cu alloy with commercial name "Gilding metal" having composition Cu: 95% & Zn: 5%, from Alpha Aesar (USA) is chosen as a target material. The circular-shaped target of diameter 20 mm and thickness of 10 mm are used for laser irradiation. Samples were mounted on rotating target holder inside a vacuum chamber to achieve fresh surface for each exposure. The chamber was evacuated to the residual base pressure of 10^{-3} Torr by using a rotary pump. Two square-shaped permanent neodymium magnets 5 cm × 5 cm were used to achieve a magnetic field of strength 1.1 Tesla. Magnetic field strength was measured by Gauss meter (GM07 HIRST Magnetic Instruments Ltd. UK). The distance between the magnets was kept constant. After passing from the focusing lens of 50 cm laser beam hits the target material at an angle of 90° with respect to the surface and generates plasma. The laser irradiance was varied by varying the laser pulsed energy through software by changing Q-switch delay. The focal spot of the laser at the target surface was 955 μm which was measured by SEM analysis.

The magnetic field was employed in such a way that direction of magnetic lines of forces is perpendicular to the expansion of LPP. After laser irradiation, the breakdown of material takes place and which is captured by an optical fiber. The emission spectra were collected by using a LIBS spectrometer system (LIBS 2500 plus) in the wavelength range of 200–980 nm with a spectral resolution of 0.1 nm. To analyze the data OOLIBS software (Ocean Optics, USA) was used. The chamber was filled with ultra-pure (99.999%) Ar, Ne, and He gas turn by turn at a constant optimized pressure of 5 Torr and pressure measurement was done by using a precise pressure gauge.

Two sets of experiments were carried out:

(i) For LIBS studies, the first sets of experiment were performed at three ambient environments of Ar, Ne, and He in the presence and the absence of field. Initially these ambients were filled at optimized pressure of 5 Torr in the chamber. The Cu-alloy was exposed to single laser pulse at six various pulsed energy ranging from 75 to 200 mJ which correspond to laser irradiance ranging from 1.9 to 5 GW/cm^2.

(ii) In the second set of experiments, in order to explore magnetic field effect on surface modifications of laser-irradiated Cu-alloy by SEM analysis, the Cu targets were exposed to a 200 laser pulses at two pulsed energy 125 and 175 mJ corresponding to laser irradiance of 3.2–4.4 GW/cm^2. These two irradiances were selected after LIBS analysis optimization where maximum T_{exc} and n_e were achieved for Cu plasma under different environments of Ar, Ne, and He at a pressure of 5 Torr.

Results and discussion

In this work, we have performed experiments under vacuum and in ambient environments of inert gases Ar, He, and Ne as well in the presence as well as in the absence of magnetic field. Figure 2 depicts the emission intensity of Cu lines in the absence of field (dotted line) as well as in the presence of field (solid line) in a spectral range of 200–980 nm at an irradiance of 4.4 GW/cm^2 under vacuum condition; whereas Figure 3 depicts the overall emission intensities of spectra in the range of 200–980 nm at an irradiance of 4.4 GW/cm^2 at 5 Torr pressure of Ar. Our spectroscopic results depict that most of the species emitted by LPP of Cu in the present experimental conditions are excited neutral Cu (I) as well as singly charged emission lines of Cu (II). In overall spectra, we have labeled ten strong emission lines of neutral Cu (I) along singly ionized Cu (II). Five strong emission lines of neutral Cu (I) are chosen and their corresponding wavelength are 324.59, 393.14, 577.99, 706.55, and 817.91 nm. We have also detected singly ionized emission lines of Cu (II) and their corresponding wavelengths are 521.54, 589.20, 777.06, 801.34, and 810.90 nm. From the comparison of the emission intensities of both Cu (I) and Cu (II) lines in the presence and absence of magnetic field, it is revealed that the magnetic field has effectively reduced emission intensities of both Cu (I) as well as Cu (II) lines, but more reduction is observed in case of neutral Cu (I). This reduction is observed in the presence of background gases as well as under vacuum condition. It implies that magnetic field employment for Cu plasma is responsible for reduction of emission lines in all cases. For the sake of elucidating more comprehensive comparison a percentage decrease for both neutral Cu (I) and

https://doi.org/10.1017/S0263034618000137 Published online by Cambridge University Press

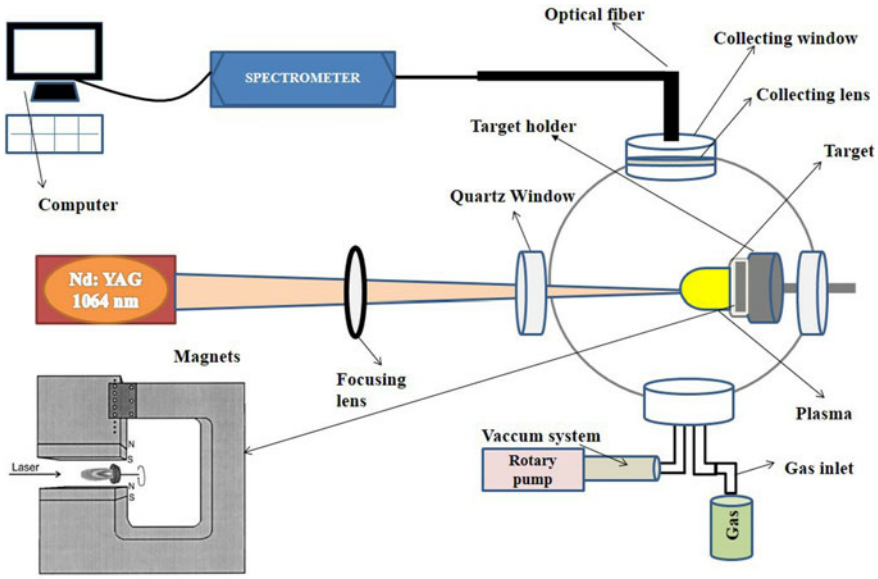

Fig. 1. The schematic of the experimental setup for investigation of magnetic field effect on laser-induced breakdown spectroscopy of Cu-alloy plasma.

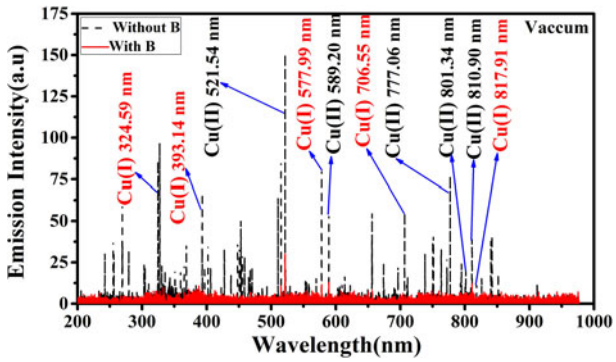

Fig. 2. The overall emission spectra of selected Cu lines obtained at an irradiance of 4.4 GW/cm^2 under vacuum in the absence and presence of magnetic field.

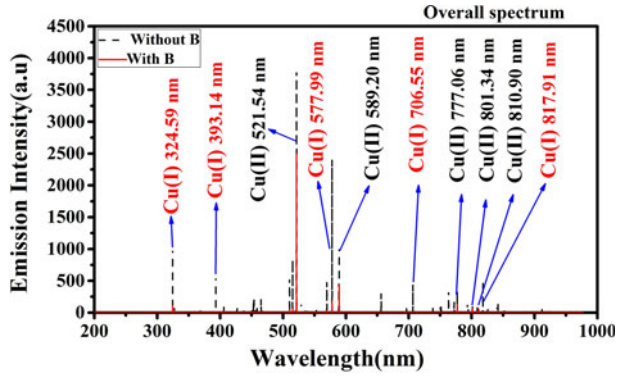

Fig. 3. The overall emission spectra of selected Cu lines obtained at an irradiance of 4.4 GW/cm^2 under Ar at a pressure of 5 Torr in the absence and presence of magnetic field.

singly ionized Cu (II) the presence of magnetic field is evaluated and is exhibited in Table 1. It is clear from Table 1 that the emission intensities of all spectral lines of both Cu (I) and Cu (II) are significantly reduced in the presence of magnetic field, but this decrease is more significant in case of neutral Cu (I). As the reasonable emission intensity is highly important for spectroscopic evaluations, therefore, we decided to select emission spectral lines of singly ionized Cu (II) for Boltzmann plot for the evaluation of both excitation temperature and electron density of Cu plasma. The emission intensities spectra of selected singly ionized Cu (II) lines are shown in Figure 4 in all environmental conditions.

Effect of magnetic field on plasma parameters of Cu-alloy at various irradiances

(i) Emission intensity

Graphs of Figure 5(a–c) correspond to variation in emission intensity of selected lines of Cu-alloy in the absence of magnetic field where graphs of Figure 5(d–f) are the corresponding variation in emission intensities of Cu-alloy in the presence of magnetic field. All the measurements are performed under different environments of Ar (a & d), Ne (b & e), and He (c & f) at a pressure of 5 Torr at various irradiances. In the field-free case, the spectral intensity initially increases and achieves its maxima at an irradiance of 4.4 GW/cm^2 then it decreases for the highest irradiance. It is also observed that emission intensity in the presence of magnetic field is significantly reduced as compared with the field-free case. It is true for all environments.

The emission intensity in Ar is maximum and follows a decreasing trend for Ne and then for He.

(ii) Excitation temperature

The T_{exc} has been evaluated by employing the Boltzmann plot method on spectroscopic data (Harilal *et al.*, 1998*a*). By assuming plasma in local thermodynamic equilibrium (LTE), the Boltzmann plot of $\ln\left((\lambda_{mn}\, I_{mn})/(g_{mA_{mn}})\right)$ versus E_m, on the spectral data gives a straight line and its slope is equal to $-1/KT_{exc}$ where λ_{mn}, I_{mn}, g_m, A_{mn}, and E_m are the wavelength, intensity of the upper energy state m, statistical weight, transition probability, and energy of upper state, respectively (Dawood *et al.*, 2015). The Boltzmann plot of selected lines is given in Figure 6. The related spectroscopic parameters used for calculation of plasma parameter are obtained from NIST database & Atomic line list

https://doi.org/10.1017/S0263034618000137 Published online by Cambridge University Press

Table 1. Comparison of percentage (%) decrease in emission intensity in the absence and presence of magnetic field

Serial no	Wavelength (nm)	Emission intensity in the absence of field	Emission intensity in the presence of field	Percentage (%) decrease in emission intensity in the presence of magnetic field
Cu (I)				
1	324.59	1000.8	105.3	89.39
2	393.14	566.8	48.3	91.47
3	577.99	2394.9	179.55	92.50
4	706.55	432.75	36	91.68
5	817.91	495.55	14.05	97.16
Cu (II)				
1	521.54	3793	2500	34.08
2	589.20	1025.9	432.55	57.83
3	777.06	332.15	125	62.36
4	801.34	141.15	63	55.36
5	810.90	95.55	55.95	41.44

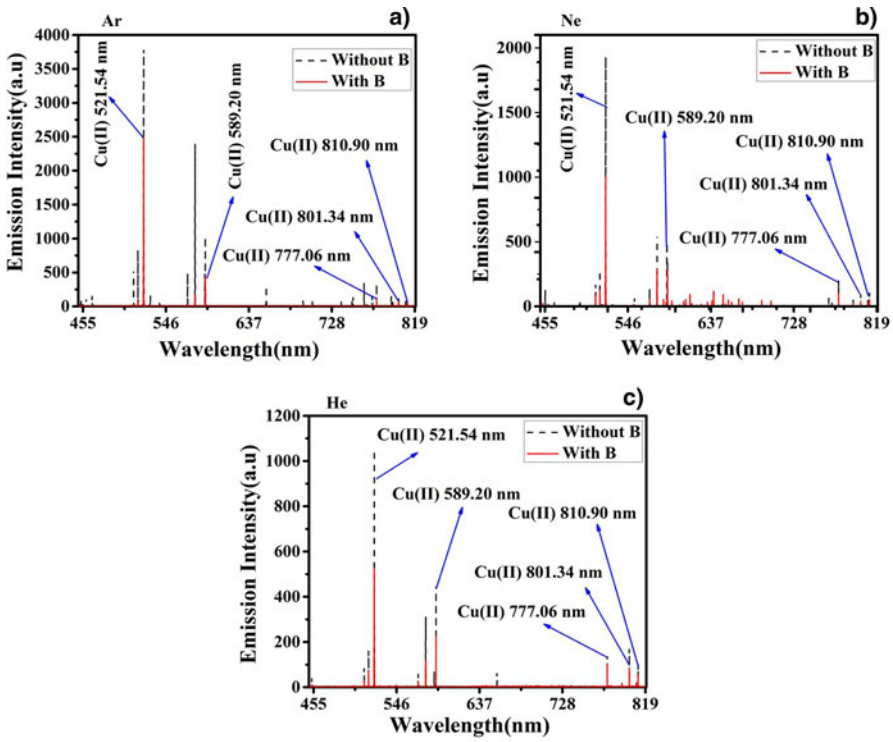

Fig. 4. Laser-induced breakdown spectra of Cu-alloy plasma obtained at an irradiance of 4.4 GW/cm^2 under the Ar, Ne, and He environments at a pressure of 5 Torr in the absence and presence of magnetic field.

(List; Kaufman and Martin 1990; Reader *et al.*, 1980) and are tabulated in Table 2.

Graphs of Figures 7 and 8 illustrate the variation in the evaluated values of T_{exc} of Cu-alloy plasma for various laser irradiance ranging from 1.9 GW/cm^2 to 5 GW/cm^2 under Ar, Ne, and He in the absence of magnetic field (Fig. 7) and presence of magnetic field (Fig. 8). In the field-free case T_{exc} of Cu-plasma varies from 7254 to 10366 K for Ar, from 6228 to 9403 K for Ne, and from 5236 to 8922 K for He; whereas with magnetic field employment, T_{exc} varies from 11843 to 14 848 K for Ar from 11 452 to 13 859 K for Ne, and from 11 196 to 12 318 K for He. In the absence and presence of field under all environments T_{exc} increase with increasing laser irradiance and achieves its maxima at 4.4 GW/cm^2. Afterward T_{exc} decreases for the highest irradiance of 5 GW/cm^2 in all ambient environments.

(iii) Electron number density

The n_e of the Cu-alloy plasma is evaluated by Stark broadening mechanism by employing following mechanism (Shaikh *et al.*, 2007).

$$\Delta\lambda_{1/2} = 2\omega\left(\frac{N_e}{10^{16}}\right) + 3.5A\left(\frac{N_e}{10^{16}}\right)^{1/4}\left[1 - 1.2N_D^{-1/3}\right] \times \omega\left(\frac{N_e}{10^{16}}\right), \quad (1)$$

https://doi.org/10.1017/S0263034618000137 Published online by Cambridge University Press

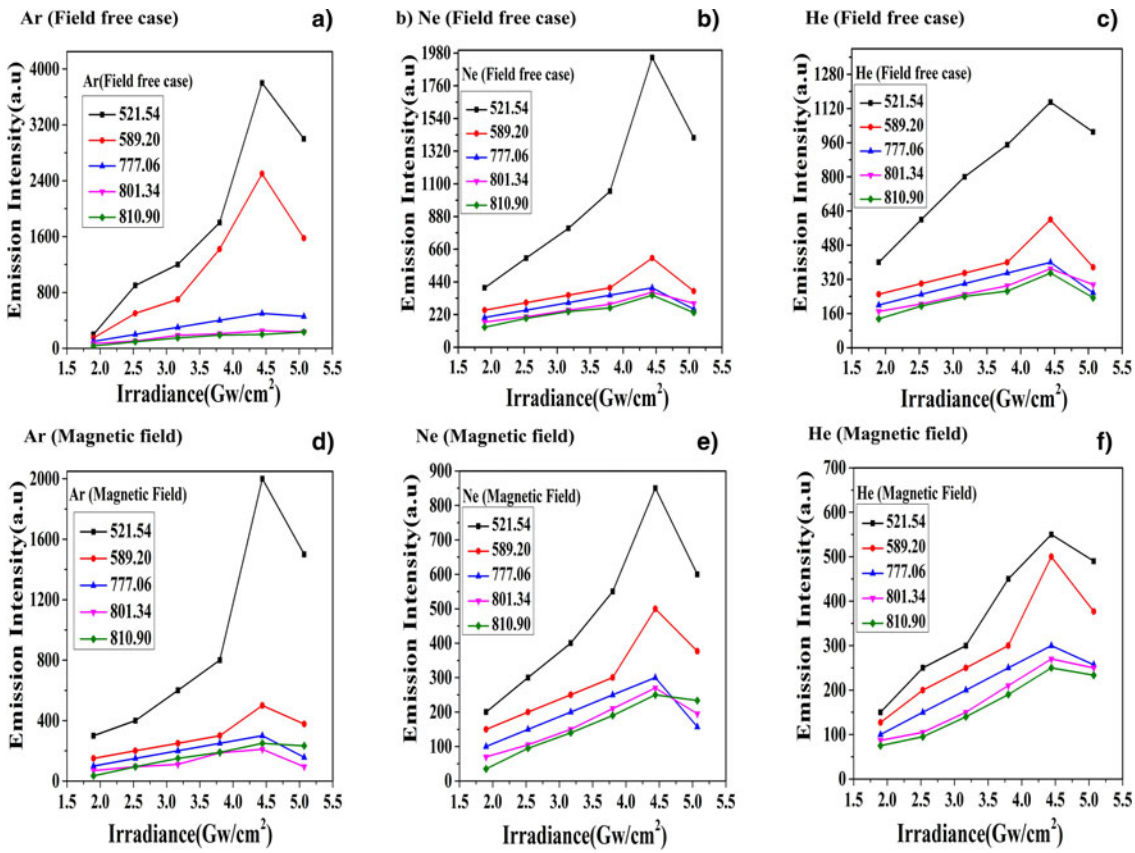

Fig. 5. The variation in emission intensity of the laser-induced Cu-alloy plasma at various irradiance under Ar, Ne, and He environments at a 5 Torr pressure in the absence and presence of magnetic field.

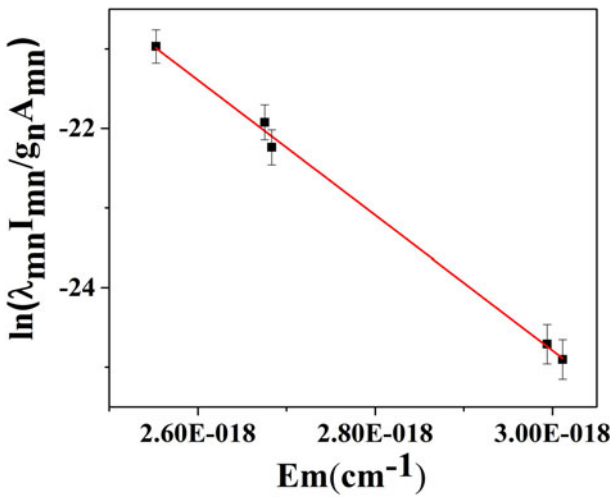

Fig. 6. The slope of Boltzmann plot obtained by using spectroscopic data of laser-ablated Cu.

where $\Delta\lambda_{1/2}$ is the full-width at half-maximum of the spectral line having a wavelength of 521.54 nm, ωis the electron impact width parameter and A is the ion broadening parameter. Where N_D is the number of particles in the Debye sphere and can be calculated by the following relation (Shaikh *et al.*, 2007):

$$N_D = 1.72 \times 10^9 \frac{T_e^{3/2}(\text{eV})}{N_e^{1/2}(\text{cm}^{-3})}. \quad (2)$$

In our case, ion-broadening is negligible (Dawood *et al.*, 2015); therefore Eq. (3) reduces to,

$$\Delta\lambda_{1/2} = 2\omega\left(\frac{N_e}{10^{16}}\right). \quad (3)$$

The Cu (II) line of 521.54 nm wavelength is used for the calculation of n_e. The selected line must be sharp as well as least broadened and fulfill the necessary criteria that it is not self-absorbed. The self-absorption coefficient for 521.54 nm line may be calculated (Sherbini *et al.*, 2012; Cristoforetti *et al.*, 2010)

$$SA = \frac{I(\lambda_o)}{I_o(\lambda_o)} = \left[\frac{n_e}{n_e^{H\alpha}}\right]^{1/\alpha}, \quad (4)$$

where I (λ_o) is the spectral intensity of standard line with negligible self-absorption and I_o (λ_o) is the spectral intensity of experimentally measured line. n_e and $n_e^{H\alpha}$ are the number density of line under investigation and the number density of H_α line, respectively; whereas the value of α is −0.54. The calculated

https://doi.org/10.1017/S0263034618000137 Published online by Cambridge University Press

Table 2. Spectroscopic parameters of Cu II lines obtained by NIST Database and literature [19–21]

Wavelength (nm)	Transitions	Terms	Energy of upper level E_m (cm^{-1})	Statistical weight (gm)	Transition probabilities (10^8 S^{-1})
521.54	$3d^{10}.9p \rightarrow 3d^9.4s.(^3D).7s$	$3G–3F^o$	134 742.85	9	2.13×10^{-4}
589.20	$3d^9.4d \rightarrow 3d^8.(^3P).4s.4p.(^3P^o)$	$1D–3P^o$	135 135.16	3	4.92×10^{-4}
777.06	$3d^8.(^3F).4s.4p.(^1P^o) \rightarrow 3d^9.(^2D_{5/2}).8s$	$3D^o–(5/2,1/2)$	150 782.42	5	3.05×10^{-3}
801.34	$3d^9.4d \rightarrow 3d^8.(^1D).4s.4p.(3P^o)$	$3D–3F^o$	128 559.31	7	1.97×10^{-4}
810.91	$3d^9.6p \rightarrow 3d^9.7d$	$3D^o–3P$	151 662.97	5	1.13×10^{-2}

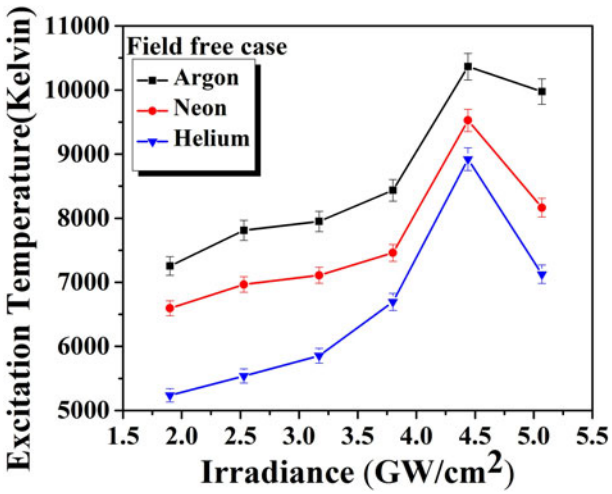

Fig. 7. The variation in excitation temperature of laser-induced Cu-alloy plasma at various irradiance under Ar, Ne, and He environment at a 5 Torr pressure in the absence magnetic field.

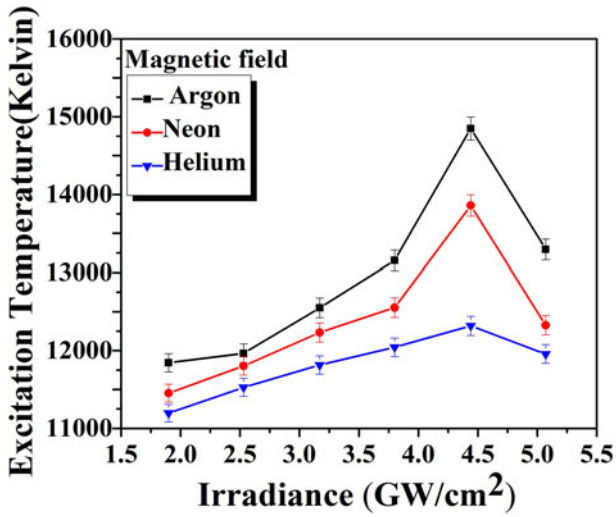

Fig. 8. The variation in excitation temperature of laser-induced Cu-alloy plasma at various irradiances under Ar, Ne, and He environment at a 5 Torr pressure in the presence of magnetic field.

value of *SA* is nearly equal to 1 that is for optically thin line and therefore is not affected by plasma in homogeneity giving negligible self-absorption effects (Hayat *et al.*, 2016).

Validity of LTE

For the validity of LTE a Mc Whirter's criterion should be fulfilled which is given by following relation (Singh and Sharma, 2017)

$$n_e \geq 1.6 \times 10^{12} T^{1/2} (\Delta E)^3. \quad (5)$$

Using Eq. (5), we have deduced that $n_e \sim 2.53 \times 10^{15}$ cm^{-3}. By substituting $T_{exc} =$ 14 848 K, for Cu-plasma in Ar experimentally calculated n_e is of the order of 10^{18} cm^{-3} which is much higher and it confirms the validity of LTE.

Graphs of Figures 9 and 10 illustrate the variation in the evaluated values of n_e of Cu-alloy plasma for various laser irradiance ranging from 1.9 to 5 GW/cm^2 under Ar, Ne, and He in the absence of magnetic field (Fig. 9) and presence of magnetic field (Fig. 10). In the field-free case n_e of Cu-plasma varies from 1.35×10^{18} to 1.80×10^{18} (cm^{-3}) for Ar, from 1.10×10^{18} to 1.75×10^{18} (cm^{-3}) for Ne, and from 1.05×10^{18} to 1.62×10^{18} (cm^{-3}) for He. In magnetic field employment, it varies from 1.38×10^{18} to 1.92×10^{18} (cm^{-3}) for Ar, from 1.12×10^{18} to 1.80×10^{18} (cm^{-3}) for Ne, and from 1.07×10^{18} to 1.66×10^{18} (cm^{-3}) for He. In the presence as well as the absence of TMF under all environments n_e increase with increasing laser irradiance and achieves its maxima at 4.4 GW/cm^2. Afterward n_e decreases for the highest irradiance of 5 GW/cm^2 in all ambient environments.

Discussion

This initial increase in emission intensity of Cu-alloy plasma with increasing laser irradiance from 1.9 to 4.4 GW/cm^2 is attributable to enhance the ablation rate, collisional excitation/de-excitation, and spatial confinement of plasma (Harilal *et al.*, 1998*b*; Hafeez *et al.*, 2008; Amin *et al.*, 2017). There are several groups who reported an increase in emission intensity by applying external magnetic field (Li *et al.*, 2009; Cheng *et al.*, 2015; Singh and Sharma, 2016; Creel and Lunney, 2018). Although in recent era, there are a lot of groups who reported a significant decrease in emission intensity by applying external magnetic field like Harilal *et al.* (2004) reported significant decrease in Al (I) and Al (II) intensity by applying external magnetic field. Another group reported the decrease in emission intensity in LPP of Cobalt by applying an external magnetic field of 0.8 T (Shen *et al.*, 2006). Iftikhar *et al.* (2017) reported the decrease in emission intensity of LPP of Ge in the presence of external magnetic field as compared with the field-free case. Joshi *et al.* (2010) investigated the LPP of Li in the presence of magnetic field and their

https://doi.org/10.1017/S0263034618000137 Published online by Cambridge University Press

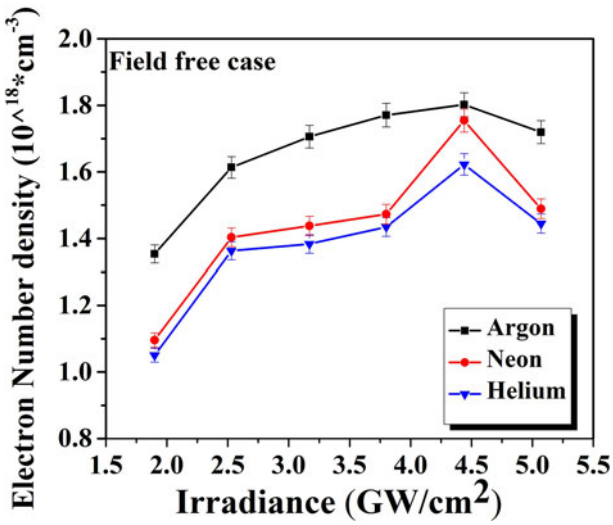

Fig. 9. The variation in electron number density of laser-induced Cu-alloy plasma at various irradiances under Ar, Ne, and He environments at a 5 Torr pressure in the absence magnetic field.

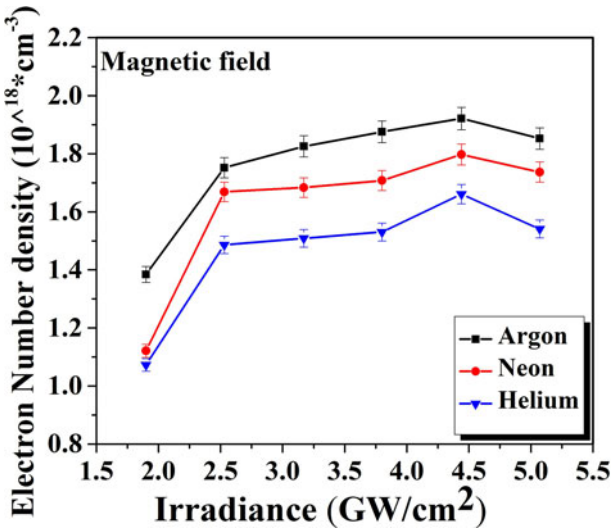

Fig. 10. The variation in electron number density of laser-induced Cu-alloy plasma at various irradiances under Ar, Ne, and He environments at a 5 Torr pressure in the presence of magnetic field.

study depicted the decrease in emission intensity of some selected lines of Li (I) and for all selected lines of Li (II). Kim *et al.* (2007) reported the decrease in emission intensity of Zn (I) during their investigation of LPP of Zn for ZnO films grown by pulsed laser deposition.

Various research groups reported that various mechanisms are responsible for increase or decrease in emission intensity by applying external magnetic field such as an increase in ionization, increase/decrease in effective plasma density, increased/decreased radiative recombination, and increase/decrease in both confinement and radiative recombination. The nature of target material also contributes for enhancement of emission intensity (Harilal *et al.*, 2004; Shen *et al.*, 2006; Kim *et al.*, 2007; Li *et al.*, 2009; Joshi *et al.*, 2010; Cheng *et al.*, 2015; Singh and Sharma, 2016; Iftikhar *et al.*, 2017).

In our experiment, it is revealed that emission intensity of Cu (II) line remains almost half in the presence of magnetic field employment. Reduction in emission intensity is attributable to a reduction in lifetime of upper state of Cu plasma. The lowering in upper state lifetime is attributable to pronounced magnetic confinement effect. When the magnetic field confines the plasma and free expansion of plasma is restricted, the interaction time for recombination is very much reduced. As a result emission intensity is reduced (Shen *et al.*, 2006; Joshi *et al.*, 2010). This decrease in emission spectra of Cu (I) and Cu (II) is also due to decrease in the radiative recombination process and increase in the three-body radiative recombination process. When the laser pulse is over, the charge composition of the plasma is governed by a three-body recombination, which dominates over radiative and/or dielectronic effects due to the rapid drop in T_{exc}. As the plasma expands, the interaction time for recombination is very much reduced as a result emission intensity reduces in the presence of a magnetic field as compared with the field-free region (Harilal *et al.*, 2004; Shen *et al.*, 2006).

The rates for three-body (R_c) and radiative (R_r) recombination are related to density and temperature of the plasma through following relations (Harilal *et al.*, 2011);

$$R_c = -9.2 \times 10^{-23} \times Z^3 \times \ln\sqrt{Z^2+1} \times T_{exc}^{9/2} \times n_e^2 \times n_i, \quad (6)$$

$$R_r = -2.7 \times 10^{-19} \times Z^2 \times T_{exc}^{-3/4} \times n_e \times n_i, \quad (7)$$

where T_{exc} is in eV and n_e is in m^{-3}. From Eqs (6) and (7), the three-body recombination will dominate over radiative recombination if it follows the following relation (Rumsby and Paul, 1974);

$$n_e \geq \frac{3 \times 10^{19} T_{exc}^{3.75}}{Z}\ m^{-3}. \quad (8)$$

Our calculated $n_e \sim 10^{24}\ m^{-3}$ although result from Eq. (8) give us $n_e \sim 10^{19}\ m^{-3}$. It implies that in the presence of field three-body recombination process dominates over irradiative recombination, which confirms the validity of three-body recombination process and it supports the argument of a decrease in emission intensity in the presence of magnetic field. Another possible reason for the rapid decline in emission intensity of Cu (I) and Cu (II) is due to transfer of energy inside the plasma and this energy transfer comprises an exchange of energy through charge exchange and impact ionization (Harilal *et al.*, 2004; Shen *et al.*, 2006).

The trend of variation in T_{exc} and n_e with increasing laser irradiance are explained below:

Initially, T_{exc} and n_e increase with the increasing laser irradiance, then later on it decreases for the highest irradiance. Initially ablation rate increases with the increase of laser irradiance due to comparatively less absorption of laser energy in the vapor volume. This increases the energy deposition in the target material. This ablation plume continues to absorb laser energy by inverse Bremsstrahlung ionization (IBI) and multi photo ionization (MPI) processes and is responsible to increase in *K.E* and n_e of Cu-plasma (Vladoiu *et al.*, 2008). The constraint of ambient gas effectively limits the free expansion of the plasma species which participate in increasing the T_{exc} and n_e of a charged particle by diminishing its expansion rate. All ambients at a pressure

https://doi.org/10.1017/S0263034618000137 Published online by Cambridge University Press

of 5 Torr are found to be sufficient to confine LPP plume. The generated LPP can absorb laser energy through two processes such as MPI and IBI. The IBI is estimated using the relation (Chang & Warner, 1996).

$$\alpha_{IB} \approx 1.37 \times 10^{-35} \times \lambda^3 \times n_e^2 \times T_{exc}^{-1/2}, \quad (9)$$

where λ (μm) is the wavelength of the laser, T_{exc} (K), and n_e (cm^{-3}). It depends upon wavelength, so the absorption of laser energy by plasma is more efficiently absorbed by IBI in case of 1064 nm as compared with 532 and 355 nm lasers. And in our experimental study, we have used 1064 nm laser as an irradiation source so IBI is dominant process on MPI because of the longer laser wavelength. So we can say that IBI is the process by which LPP of Cu will continue to absorb laser energy (Harilal *et al.*, 1997). Reflection of laser light depends upon laser frequency and plasma frequency. For reflection of incoming laser radiation by LPP, plasma frequency should be greater than or equal to laser frequency. The plasma frequency can be estimated by following relation (Huba, 2016).

$$\omega_p = 8.98 \times 10^3 \times n_e^{1/2} \text{ Hz}, \quad (10)$$

where ω_p is the plasma frequency (Hz), and n_e (cm^{-3}). By substituting $n_e = 1.92 \times 10^{18}$ cm^{-3}, we have deduced that $\omega_p = 1.24 \times 10^{13}$ Hz. It shows that plasma frequency is slightly lower than the laser frequency which is 2.82×10^{14} Hz for Nd: YAG laser (1064 nm) (Harilal *et al.*, 1997). It suggests that the laser light is not completely reflected but it is absorbed in plasma (not specimen but in plasma). As the laser irradiance is further raised from the relevant maxima, both T_{exc} and n_e decrease that is due to plasma plume shielding effect (Akram *et al.*, 2014).

From graphs of Figures 7–10, it is clear that T_{exc} and n_e are enhanced in the presence of magnetic field. This enhancement is also due to magnetic confinement of the LIP. The plume expands freely in field-free case as compared with magnetic field employment because plume expansion happens freely without a field. As it expands across a field, the plume front decelerates in the direction normal to the target surface (Amin *et al.*, 2017). Magnetic pressure tries to stop plume but instead of that plume diffuses across the magnetic field. The plume aims to develop along the lines of magnetic pointing lateral expansion. Radial expansion velocity of plasma is lower as compared with the peak expansion velocity in the axial direction which is perpendicular to the specimen (Harilal *et al.*, 2004). When the plasma pressure becomes higher than the magnetic pressure, the plasma is probably going to enter through the region involved by the magnetic field. When plasma pressure becomes equal to magnetic pressure, then plasma confinements occur which results into stagnation. In this case, the collisional frequency of charged species is enhanced which is depicted to confine the plasma to a smaller region in addition to enlarging their oscillation frequency. Thus, restriction of the cross-field expansion by the magnetic field outcomes the thermalization and high pressure in the confined plasma (Amin *et al.*, 2017).

The enhancement of T_{exc} in the presence of magnetic field is ascribed to phenomenon such as resistive Ohmic/Joule heating and adiabatic pressure. According to this MHD model, the generalized form of Ohm's law is given by (Boyd and Sanderson, 2003)

$$E + V \times B = J/\sigma_o + J \times B/n_e e, \quad (11)$$

where E and B are the electric and magnetic fields, V the mass flow velocity, J the electron conduction current, and σ_0 the conductivity. First term explains the expansion of LPP inside a magnetic field and it can be employed by using the MHD model. At the point when the LPP extends crosswise over the field, then electrons gain energy from *K.E* of the plume. This gain in energy is due to work done against the $J \times B$ term that acts to slow down the flow. As a result of this work done, plasma will heat up. The force of $J \times B$ drives the LPP till magnetic pressure become equal with LPP pressure. This prompts the Joule heating of the electrons with the goal that electrons can keep on exciting higher-charge states. So the magnetic field accelerates electron collisional ionization, which enhances the number density of the charged particles.

One of the key parameters for expansion into a magnetic field is the thermal β_t. The thermal β_t of the plasma is given by (Iftikhar *et al.*, 2017).

$$\beta_t = \frac{8\pi n_e K T_{exc}}{B^2}, \quad (12)$$

where B is the magnetic field (G), n_e (cm^{-3}), k is the Boltzmann constant, and T_{exc} (eV). When plasma pressure is balanced with LPP pressure then the expansion of the plume will stop or $\beta = 1$. Under the effect of thermal beta, the deceleration of the plasma development can be given as (Waheed *et al.*, 2017)

$$V_2/V_1 = \left(1 - \frac{1}{\beta}\right)^{1/2}. \quad (13)$$

In this equation, V_1 and V_2 are the velocities of plasma species in the absence and presence of field respectively. When $\beta > 1$ then there will be no magnetic confinement but if $\beta < 1$ then there will be magnetic confinement. When the kinetic pressure exerted by plasma becomes greater as compared with pressure employed by magnetic field then LPP will penetrate inside the field. Due to this penetration magnetic field exercises more resistance to plasma evolving that causes the decline in pressure inside the plume. If this kinetic pressure is balanced by pressure exerted by field then compression, as well as confinement of LPP is observed. The variation of β_t with increasing irradiances is tabulated in Tables 3–5 in all ambients of Ar, Ne, and He, respectively. These values are also drawn graphically in Figure 11 to depict a variation of thermal beta in accordance with irradiance. The maximum value of thermal β_t is achieved at an irradiance of 4.4 GW/cm^2 where maximum T_{exc} and n_e of Cu-plasma is achieved for all environments.

It is reported in the literature (Harilal *et al.*, 2004) that plume is not completely stopped by magnetic field employment although its speed is slowed down considerably. So β_t is not only decisive factor but an additional important parameter to describe plasma confinement is directional β_d.

After the initial conversion of thermal energy into directed energy, β_d is given by

$$\beta_d = \frac{4\pi n_e (3K_B T_{exc})}{B^2}, \quad (14)$$

where B (G), n_e (cm^{-3}), and T_{exc} (eV). The directed β_d is evaluated for different values of n_e and T_{exc} of the Cu-alloy plasma at various irradiances for all environmental conditions. The value of magnetic pressure is always higher than plasma pressure,

https://doi.org/10.1017/S0263034618000137 Published online by Cambridge University Press

Table 3. Evaluated values of excitation temperature, electron number density, thermal beta, directional beta, and diffusion time for laser-irradiated Cu plasma in Ar environment at different values of irradiances in the presence and absence of magnetic field

Irradiance (GW/cm^2)	Excitation temp (Kelvin) (field-free case)	Excitation temp (magnetic field) (Kelvin)	n_e (10^{18} cm^{-3}) (field-free case)	n_e (10^{18} cm^{-3}) (magnetic field)	Thermal beta	Directional beta	Diffusion time (ns) (magnetic field)
(Argon)							
1.9	7253.79019	11 843.32971	1.35371	1.38439	0.47	94	238
2.5	7811.49976	11 965.31924	1.61353	1.75193	0.601	120	295
3.2	7949.17097	12 549.75098	1.70558	1.8255	0.657	131	367
3.8	8434.53254	13 155.01967	1.77069	1.87561	0.707	141	443
4.4	10 366.10921	14 847.91577	1.80188	1.92154	0.818	164	583
5.0	9975.75274	13 295.54315	1.71935	1.85238	0.706	141	543

Table 4. Evaluated values of excitation temperature, electron number density, thermal beta, directional beta, and diffusion time for laser-irradiated Cu plasma in Ne environment at different values of irradiances in the presence and absence of magnetic field

Irradiance (GW/cm^2)	Excitation temp (Kelvin) (field-free case)	Excitation temp (Kelvin) (magnetic field)	n_e (10^{18} cm^{-3}) (field-free case)	n_e (10^{18} cm^{-3}) (magnetic field)	Thermal beta	Directional beta	Diffusion time (ns) (magnetic field)
(Neon)							
1.9	6228.45965	11 452.95588	1.09594	1.12111	0.368	73.6	225
2.5	6629.74429	11 802.55097	1.40306	1.66872	0.565	113	289
3.2	6786.2043	12 233.45474	1.43736	1.68365	0.59	118	352
3.8	7163.42436	12 553.12073	1.47298	1.70796	0.615	123	413
4.4	9403.20986	13 858.84983	1.75446	1.79753	0.714	143	527
5.0	7927.63842	12 327.86041	1.48889	1.73703	0.614	123	487

Table 5. Evaluated values of excitation temperature, electron number density, thermal beta, directional beta, and diffusion time for laser-irradiated Cu plasma in He environment at different values of irradiances in the presence and absence of magnetic field

Irradiance (GW/cm^2)	Excitation temp (Kelvin) (field-free case)	Excitation temp (Kelvin) (magnetic field)	n_e (10^{18} cm^{-3}) (field-free case)	n_e (10^{18} cm^{-3}) (magnetic field)	Thermal beta	Directional beta	Diffusion time (ns) (magnetic field)
(Helium)							
1.9	5236.35108	11 196.77991	1.05066	1.07258	0.344	68.9	218
2.5	5538.81541	11 527.36264	1.36262	1.4862	0.491	98.2	277
3.2	5853.81319	11 814.61638	1.38336	1.50877	0.511	102	333
3.8	6694.85468	12 042.9522	1.43443	1.53046	0.528	106	386
4.4	8921.83497	12 318.28133	1.62239	1.66084	0.586	117	444
5.0	7126.15852	11 956.59312	1.44441	1.541	0.528	106	463

which confirms the validity of magnetic confinement. The variation of the directional beta of Cu plasma with increasing irradiances is tabulated in Tables 3–5 under all ambients of Ar, Ne, and He, respectively. These values are also drawn graphically in Figure 12 to depict a variation of directional beta in accordance with irradiance. When initially plasma starts to expand, β_d is of the order of few hundred, pointing out that LIP of Cu-alloy is in diamagnetic regime (Peyser *et al.*, 1992). The LPP diamagnetic cavity extends up to entire expelled magnetic energy is balanced to whole plasma energy. Due to the combined effect of magnetic pressure along pressure exerted by the ambient gas, this LPP will be decelerated.

We can deduce the confinement radius by assuming that plasma expands spherically, a region where the magnetic field has exerted its confinement to the plasma. The confinement radius can be deduced by using following relation (Singh and Sharma, 2017).

$$R_b = \left(\frac{3F_{la}A_l}{2\pi\left(B^2/2\mu_o + P_{air}\right)}\right)^{1/3}, \tag{15}$$

where F_{la} is absorbed laser fluence. In our case, for 1064 nm when the reflectance is 97% for Cu-alloy and for laser fluence

https://doi.org/10.1017/S0263034618000137 Published online by Cambridge University Press

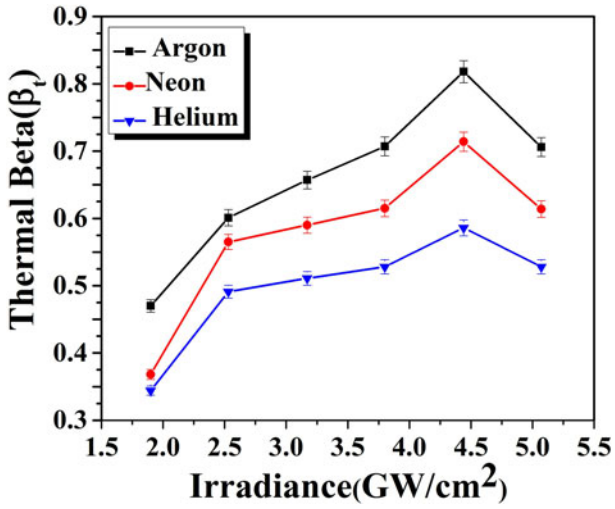

Fig. 11. The variation in thermal beta of laser-induced Cu-alloy plasma at various irradiances under Ar, Ne, and He environments at a 5 Torr pressure.

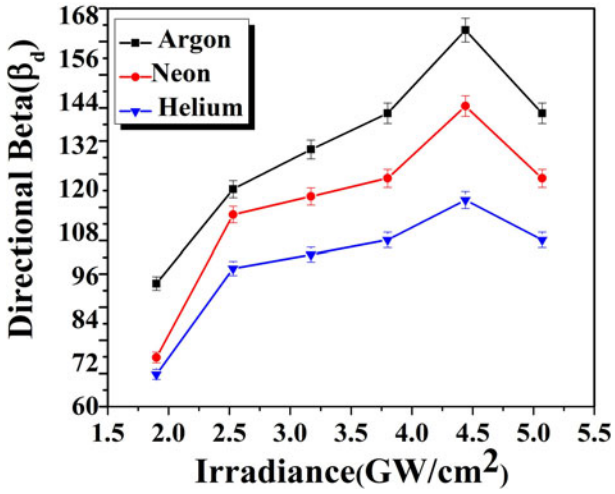

Fig. 12. The variation in directional beta of laser-induced Cu-alloy plasma at various irradiances under Ar, Ne, and He environments at a 5 Torr pressure in the presence of magnetic field.

of 50.7 J/cm^2 F_{la} becomes 1.5 J/cm^2 and the corresponding value of the confinement radius becomes 21 mm. It employs that plasma will be decelerated significantly upto distance 21 mm correspond to laser irradiance 5 GW/cm^2. The confinement radius in the presence and absence of a field is depicted in Table 6. It is also exhibited in the form of a graph as shown in Figure 13. It is clear from the table that confinement radius is significantly reduced in the presence of magnetic field ranges from 15 to 21 mm as compared with field-free case where it varies from 62 mm to 85 mm with the variation of irradiance from 1.9 to 5 GW/cm^2. It implies that confinement radius reduces from 58 to 42% when irradiance is increased from 1.9 to 5 GW/cm^2. It clearly indicates that magnetic confinement is more significant for higher irradiances due to enhanced energy deposition, ablation rate, and melt ejections (Harilal *et al.*, 2004).

At initial stages of plasma formation charged species dissipate into the region possessed by the magnetic field. The diffusion of

Table 6. Evaluated values of confinement radius at different values of irradiances in the presence and absence of magnetic field

Irradiance (GW/cm^2)	Confinement radius (mm) (field-free case)	Confinement radius (mm) (magnetic field)
(Confinement radius)		
1.9	61.6	14.9
2.5	67.7	16.4
3.2	72.9	17.7
3.8	77.4	18.8
4.4	81.5	19.8
5.0	85.2	20.6

plasma into the magnetic field is given by Harilal *et al.* (2004):

$$D = \frac{1}{B^2 T_{\mathrm{exc}}^{1/2}}. \tag{16}$$

This relation depicts that with an increase in temperature the diffusion of plasma into magnetic field reduces and as a result plasma is decelerated significantly. In a later phase of plasma plume expansion, plasma will be cooled and as a result, magnetic field will diffuse into the boundary of plasma relatively fast. The magnetic diffusion time (t_d) is a time which is essential for the conversion of magnetic field energy into Joule heat, which is given by (Harilal *et al.*, 2004)

$$t_{\mathrm{d}} = \frac{4\pi\sigma R_{\mathrm{b}}^2}{c^2}, \tag{17}$$

where t_d is diffusion time, σ is the conductivity of plasma, which is calculated by utilizing Spitzer formula (Huba, 2016). The values of t_d are evaluated by assuming electron–ion interaction and t_d in our experimental parameters depicted in Tables 3–5 by taking $Z = 1$ and these values are also shown in Figure 14 to depict a variation of diffusion time in accordance with laser irradiances

The environmental conditions also play an important rule for influencing plasma parameters. The effect of ambient environment on plasma parameters is understandable on the principle of cascade growth. The pre-requisite for cascade growth is expressed as follows: (Iida, 1990; Farid *et al.*, 2012);

$$\frac{d\varepsilon}{dt} = \frac{4\pi^2 e^2 I \nu_{\mathrm{eff}}}{m_{\mathrm{e}} c\omega^2} - \frac{2m_{\mathrm{e}}\nu_{\mathrm{eff}} E}{M}, \tag{18}$$

where ε is the energy of the free electrons, m and e are the mass and charge of the electron, M is the mass of the background gas neutral particle and E is the energy of the first ionization stage of gas, I is the radiation intensity, ω the cyclic frequency of radiation and υ_{eff} the effective frequency of electron–neutral collisions. The term on right side depicts the rise of energy by absorbing the incoming laser pulse. This energy absorption is constant for all ambients, although its second part (E/M) plays its vital rule for explaining the effect of ambient in terms of cascade growth. E/M ratio (for Ar: 0.53, for Ne: 1.08, and for He: 6.04) is lowest for Ar moreover for Ne further for He. It employs that Ar ambient is more suitable for cascade growth than for Ne and He (Iida, 1990; Bashir *et al.*, 2012). These results depict that Ar ambient

https://doi.org/10.1017/S0263034618000137 Published online by Cambridge University Press

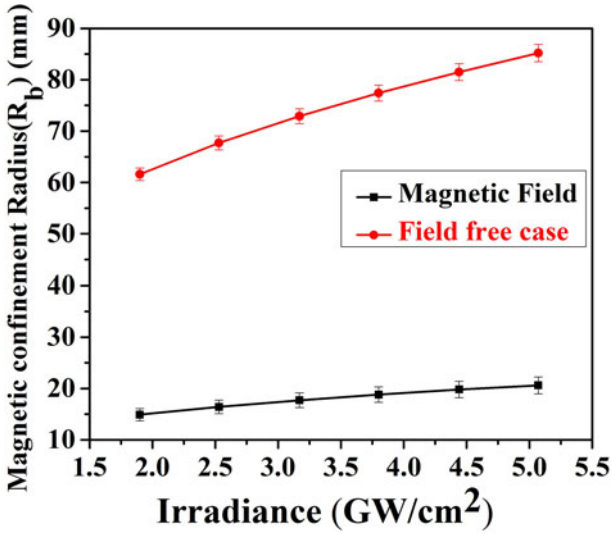

Fig. 13. The variation in magnetic confinement radius of laser-induced Cu-alloy plasma at various irradiances under Ar, Ne, and He environments at a 5 Torr pressure in the presence as well as absence of magnetic field.

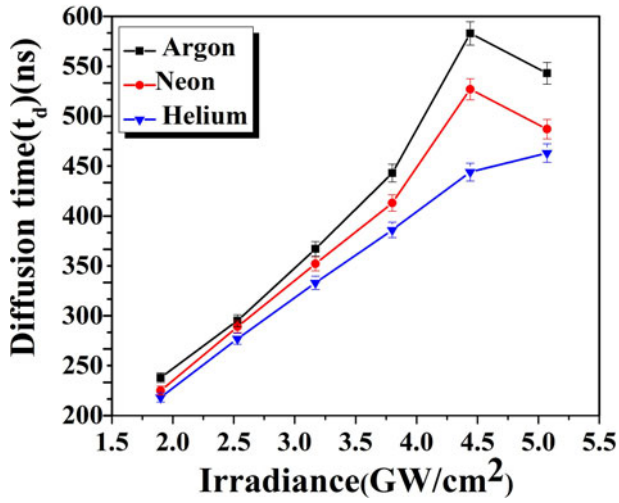

Fig. 14. The variation in diffusion time of laser-induced Cu-alloy plasma at various irradiances under Ar, Ne, and He environments at a 5 Torr pressure.

is most favorable for the highest emission intensity, T_{exc} and n_e as compared with Ne followed by He for Cu-plasma.

Another governing factor for energy loss in all ambient is thermal conductivity. The thermal conductivity influences the cascade growth in such a way that higher the thermal conductivity, consequently more heat dissipation losses will occur near specimen surface. Consequently plasma *K.E* will be lowest for He then for Ne and highest for Ar (Bashir *et al.*, 2012).

Effect of magnetic field on the surface morphology of Cu-alloy at various irradiances

For SEM analysis we have selected only two laser irradiances to irradiate Cu-alloy target.

(a) Where moderate T_{exc} and n_e of Cu-alloy plasma are attained (Fig. 15)
(b) The second selection of micrographs corresponds to laser irradiance responsible for the maximum value of T_{exc} and n_e of Cu-alloy plasma (Fig. 16)

SEM micrographs of Figure 15 reveal peripheral ablated area of Cu-alloy exposed to 200 pulses of Nd: YAG laser at an irradiance of 3.2 GW/cm^2 under ambient environments of (a) Ar, (b) Ne, and (c) He at a pressure of 5 Torr in the field-free case. It is observed that under Ar environment irregular-shaped islands like mounds are formed. Under Ne environment the density and size of island like mounds is significantly reduced. The formation of craters is also seen in Figure 15(b). In case of Cu-ablation in He environment the density of craters is significantly reduced, whereas both distinctness and size of islands are enhanced. SEM micrographs of Figure 15 reveal the surface morphology of Cu-alloy under ambient environments of (d) Ar, (e) Ne, and (f) He at a pressure of 5 Torr in presence of magnetic field. It is observed that conical structures are formed with multiple ablative layers in Ar environment. In Ne environment small-scale conical structures and droplets are grown with significant enhanced density. When material is ablated in He-protruded mounds with conical uplifted structures are formed. It is clear that structures formed in Cu-alloy in the presence of magnetic field are more protruded as compared with field-free case. Their size, as well as their density, are also significantly enhanced. It predicts that magnetic field employment is responsible for the growth of fine and uplifted structures.

SEM micrographs of Figure 16 reveal peripheral ablated areas of Cu-alloy as exposed to 200 pulses of Nd: YAG laser at an irradiance of 4.4 GW/cm^2 under ambient environments of (a) Ar, (b) Ne, and (c) He at a pressure of 5 Torr in the field-free case. Under Ar environment, few micro-sized craters, with multiple ablative layers are observed as is depicted in Figure 16a. Figure 16b, 16c shows the formation of deep cones and large size craters, ablation channels and islands like mounds are observed after irradiation in Ne and He environment. SEM micrographs of Figure 16 reveal the surface morphology of laser-irradiated Cu-alloy under ambient environments of (d) Ar, (e) Ne, and (f) He at a pressure of 5 Torr in presence of magnetic field. The formation of large-scale islands and craters are observed as shown in Figure 16d. The cone formation is also seen under Ne environment in Figure 16e. Figure 16f reveals that under He environment, density of cones, and protrusions is reduced, whereas islands are completely vanished.

The formation of islands is due to exfoliational sputtering which in turn raises the local volume of the target which is owing to the build-up of stresses. When these stresses are relaxed then islands formation occurs due to diffusion, transformation, and aggression of primary defects. At higher laser irradiance the significant distinctness and decrease of density of islands are observed (Carriere *et al.*, 1991). The craters formation can be explained on the basis of thermal ablation which is interpreted to laser-induced heating, melting, explosive boiling, and thermal desorption of the target surface (Yousaf *et al.*, 2013). The variation in the size of craters is ascribed to the non-uniform distribution of surface defects, such as contaminants, inclusions, and small pits which are responsible for non-uniform energy distribution (Dauscher *et al.*, 1996). The formation of craters is explained in such a way that when ablation takes place at a laser irradiance greater than ablation threshold then the formation of super-heated metastable liquid takes place. This super-heated liquid

https://doi.org/10.1017/S0263034618000137 Published online by Cambridge University Press

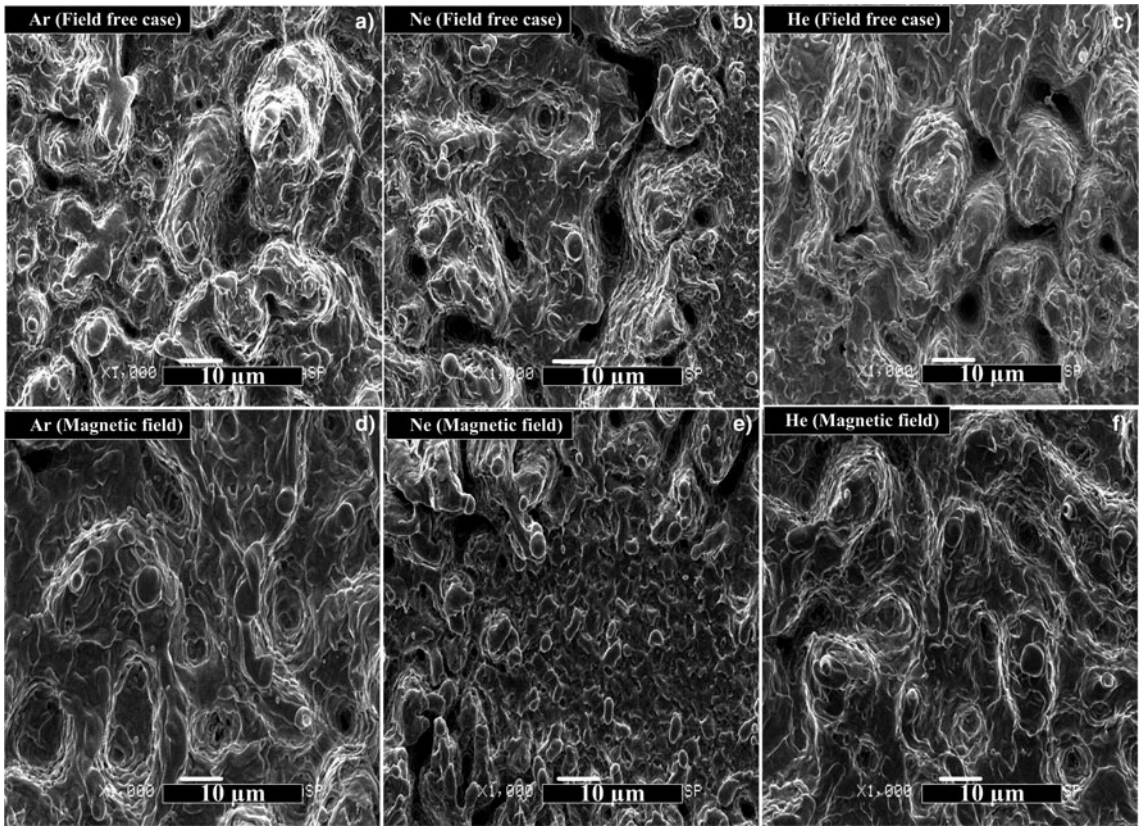

Fig. 15. SEM image revealing the surface morphology of periphery ablated area of Cu-alloy under different environments of Ar (a & d), Ne (b & e), and He (c & f) at a pressure of 5 Torr in the absence as well as presence of magnetic field respectively for irradiance of 3.2 GW/cm^2.

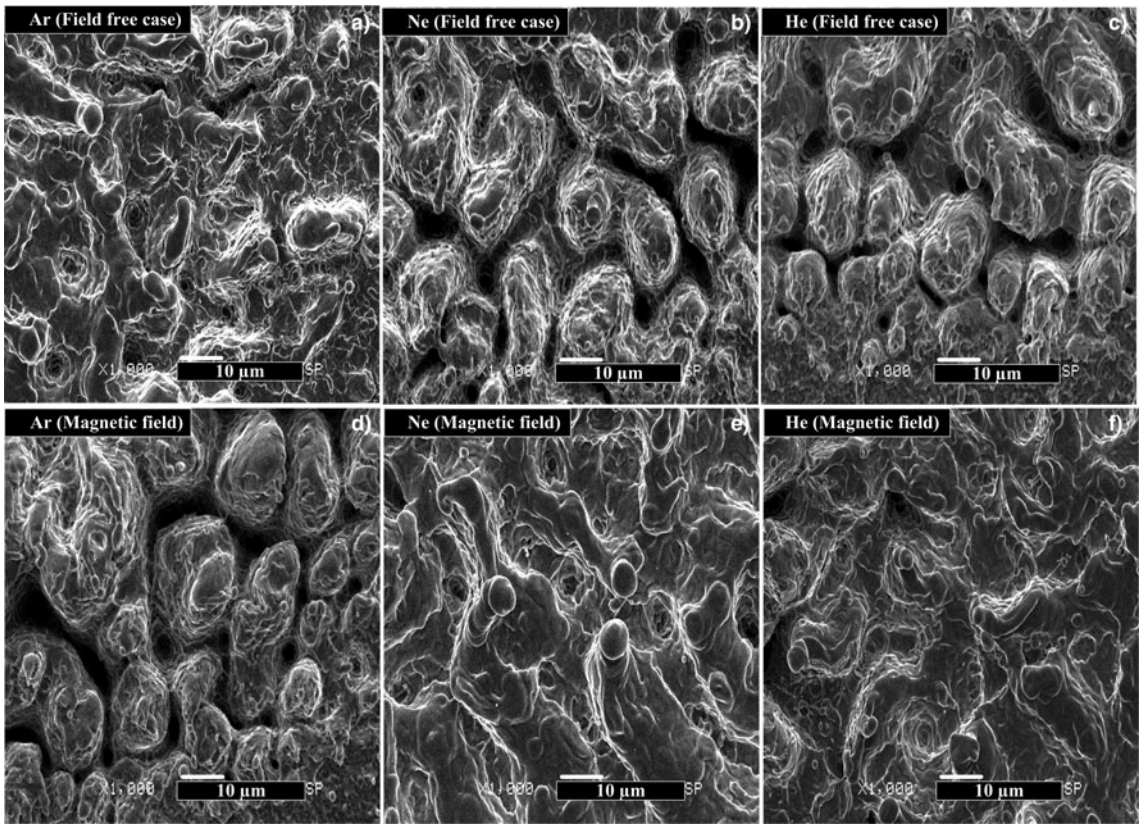

Fig. 16. SEM image revealing the surface morphology of periphery-ablated area of Cu-alloy under different environments of Ar (a & d), Ne (b & e), and He (c & f) at a pressure of 5 Torr in the absence as well as presence of magnetic field respectively for irradiance of 4.4 GW/cm^2.

https://doi.org/10.1017/S0263034618000137 Published online by Cambridge University Press

formation supports explosive boiling which is due to inhomogenous bubble nucleation. Subsequently, mechanical stresses that are generated inside the superficial layer results into explosive relaxation which becomes a cause of craters (Bashir *et al.*, 2015). Although the increase in size and density of craters is due to increase in recoil pressure by increasing laser irradiance and changing ambient environments. However, the decrease in size and density of craters is associated with redeposition of ablated material. Craters density is reduced at higher irradiance and also in the presence of magnetic field under He and Ne environment and is due to refilling of these craters by molten material (Yousaf *et al.*, 2013). Hydro-dynamic sputtering, defects, and ablation due to evaporation resistive impurities are attributed to cones formation (Dolgaev *et al.*, 2006). The density of observed cones increases with the increase in laser irradiance which is due to enhanced energy deposition. The formation of droplets is attributed to a transition from a vaporization-dominated ablation regime to a regime where melt-expulsion occurs, and "hydrodynamical" sputtering becomes dominant. This hydro-dynamical mechanism refers to the formation and liberation of micro size droplets from the melt at the surface of the material (Bleiner and Bogaerts, 2006).

The surface modifications of laser-ablated Cu-alloy are well correlated with plasma parameters such as T_{exc} and n_e. At a laser irradiance corresponding to moderate T_{exc} and n_e of Cu-plasma is due to small energy deposition from electron to the lattice and consequently, irregular shaped islands like mounds and craters are formed. When the fluence is increased from 3.2 to 4.4 GW/cm^2, the significant increase in plasma parameters is responsible for more energy deposition from electrons to the lattice which causes enhancement of the size of structures. The distinctness of islands is also increased significantly and their appearance becomes more defined. It employs that plasma parameters can control the growth of structures on the laser-ablated target.

When T_{exc} and n_e of Cu-plasma are exceeded from certain limit in environmental condition of Ar, then due to its low value of E/M(0.53) ratio, low thermal conductivity {17.72[W/(m. K)]} and high cascade growth, the structures due to over melting can be destroyed. The other possible cause is the high-density plasma (1.80×10^{18} cm^{-3}) which shields the Cu target more effectively from laser irradiations as compared with Ne and He.

The employment of magnetic field is responsible for the growth of uplifted and fine structures as compared with field-free case. Higher collisional frequency in the case of magnetic confinement is responsible for distribution of large-sized islands or mounds into smaller structures due to higher T_{exc} and n_e of charged species. After the laser–matter interaction, the collisional frequencies of plasma species are significantly enhanced by increasing the laser irradiance which is responsible for enhanced momentum transfer. The confinement of LIP by magnetic field employment as well as ambient environment also favors and supports the cascade growth which results in a significant increase in plasma parameters, that is T_{exc} as well as free n_e (Weyl, 1989). After achieving maxima in T_{exc} and n_e of free electrons, the more energy absorption by the electrons to the lattice takes place this enhanced energy deposition to lattice is responsible to break up large sized islands or mounds into smaller and fine islands like structures in the presence of magnetic field. It implies that surface modification can be governed by controlling plasma parameters as well as magnetic confinement of plasma. Argon gas pressures of 5 Torr as background gas of Cu plasma along with magnetic field strength of 1.1 Tesla offers confinement, which prevents the free expansion of the plume and random movement of an ejected material during laser ablation and stabilizes the generation of surface waves, in a well-defined manner (Ganeev *et al.*, 2010). The decrease in the size of mounds or islands can be also attributed to the presence of residual stresses and generation of defects which are significantly enhanced in the presence of magnetic confinement. The fast melting and cooling, the resolidification, and recrystallization processes start to take place and large-sized islands and mounds break up into smaller ones (Bashir *et al.*, 2015).

Conclusions

The significant effects of the transverse magnetic field on the Cu plasma parameters as a function of irradiance under ambient environments of Ar, Ne, and He are revealed. It was found that Cu plasma parameters are significantly enhanced in the presence of magnetic field as compared with field-free case at all irradiances, under ambient environments of Ar, Ne, and He. The enhancement in plasma parameters is due to magnetic confinement, Joule heating confinement, and adiabatic compression. Cu plasma parameters, that is emission intensity, T_{exc}, and n_e are found to be strongly dependent upon irradiance. The T_{exc} and n_e values initially increase, achieve their maxima and then decreases. This trend remains same for all environmental conditions. The same trends of T_{exc} and n_e are observed in the presence of magnetic field as well as field-free case under all ambients. However, for all cases emission intensities; T_{exc} and n_e values are higher in an ambient of Ar than Ne followed by He. These results are attributed to lower thermal conductivity and higher cascade growth of Ar than Ne followed by He. The values of thermal beta (β_t), directional beta (β_d), confinement radius (R_b), and diffusion time (t_d) for laser-irradiated Cu-alloy plasma are also analytically evaluated for different irradiances in all environments. For all cases, β_t is <1 which confirms the confinements of Cu plasma under 1.1 T magnetic field. The results of directional beta (β_d) confirm that LPP is in the diamagnetic regime. The evaluation result of confinement radius (R_b) proves that our LPP is constrained to the very small region as compared with field-free case which confirms the validity of magnetic confinement. For all cases, the diffusion time (t_d) is calculated. Distinct and well-defined structuring is observed in the absence of the magnetic field. Non-uniform melting and indistinct structures are observed in the presence of the magnetic field except Ar at higher irradiances where well-defined structures are observed. These structures are well correlated with plasma parameters. These structures can enhance micro hardness and corrosion resistance of Cu, which will increase its applications in canon shell industry. By controlling plasma parameters under different conditions of laser fluences and magnetic field employment the surface structuring of materials can be controlled. The magnetic field employment on LIP can be used as an energy analyzer and mass separation of ions and isotopes according to their mass to charge ratio. As the magnetic field can enhance the plasma parameters (T_{exc} and n_e), therefore makes the plasma more useful for thin-film deposition and ion implantation.

Acknowledgment. We acknowledge Higher Education Commission of Pakistan for funding the project "Strengthening of Laser Facilities at GC University Lahore". We also acknowledge Dr. Tousif Hussain for providing the SEM facility.

https://doi.org/10.1017/S0263034618000137 Published online by Cambridge University Press

References

Akram M, Bashir S, Hayat A, Mahmood K, Ahmad R and Rahman MK (2014) Effect of laser irradiance on the surface morphology and laser Induced plasma parameters of zinc. *Laser and Particle Beams* **32**, 119–128.

Amin S, Bashir S, Anjum S, Akram M, Hayat A, Waheed S, Iftikhar H, Dawood A and Mahmood K (2017) Optical emission spectroscopy of magnetically confined laser induced vanadium pentoxide (V_2O_5) plasma. *Physics of Plasmas* **24**, 083112.

Atomic line list V2.05b21. http://www.pa.uky.edu/~peter/newpage/

Bashir S, Farid N, Mehmood K and Rafique MS (2012) Influence of ambient gas and its pressure on the laser-induced breakdown spectroscopy and the surface morphology of laser-ablated Cd. *Applied Physics A: Solids and Surfaces* **107**, 203–212.

Bashir S, Khurshid S, Akram M, Ali N, Ahmad S and Yousaf D (2015) Pulsed laser ablation of Ni in vacuum and N_2 atmosphere at various fluences. *Quantum Electronics* **45**, 640.

Bleiner D and Bogaerts A (2006) Multiplicity and contiguity of ablation mechanisms in laser-assisted analytical micro-sampling. *Spectrochimica Acta B* **61**, 421–432.

Boyd TJM and Sanderson JJ. 2003 *The Physics of Plasmas*. UK: Cambridge University Press.

Carriere T, Ortiz C and Fuchs G (1991) Fractal-like aggregation of Au islands induced by laser irradiation. *Journal of Applied Physics* **70**, 5063–5067.

Chang JJ and Warner BE (1996) Laser-plasma interaction during visible-laser ablation of methods. *Applied Physics Letters* **69**, 473–475.

Cheng L, Xun G, Qi L, Chao S and Jingquan L (2015) Spectral enhancement of laser-induced breakdown spectroscopy in external magnetic field. *Plasma Science and Technology* **17**, 919.

Creel JR and Lunney JG (2018) Compression and heating of a laser-produced plasma using single and double induction coils. *Applied Physics A* **124**, 124.

Cristoforetti G, Lorenzetti G, Legnaioli S and Palleschi V (2010) Investigation on the role of air in the dynamical evolution and thermodynamic state of a laser-induced aluminium plasma by spatial- and time-resolved spectroscopy. *Spectrochimica Acta B* **65**, 787.

Dauscher A, Feregotto V, Cordier P and Thomy A (1996) Laser induced periodic surface structures on iron. *Applied Surface Science* **96–98**, 410–414.

Dawood A, Bashir S, Akram M, Hayat A, Ahmed S, Iqbal MH and Kazmi AH (2015) Effect of nature and pressure of ambient environments on the surface morphology, plasma parameters, hardness, and corrosion resistance of laser-irradiated Mg-alloy. *Laser and Particle Beams* **33**, 315–330.

Dolgaev SI, Fernández-Pradas JM, Morenza JL, Serra P and Shafeev GA (2006) Growth of large micro cones in steel under multi pulsed Nd: YAG laser irradiation. *Applied Physics A: Solids and Surfaces* **83**, 417–420.

Ducruet C, Kornilov N, de Julián Fernández C and Givord D (2006) Laser generated plasmas characterized under magnetic field. *Applied Physics Letters* **88**, 044102.

Farid N, Bashir S and Mehmood K (2012) Effect of ambient gas conditions on laser-induced copper plasma and surface morphology. *Physica Scripta* **85**, 015702–015709.

Ganeev R, Baba M, Ozaki T and Kuroda H (2010) Long-and short-period nanostructure formation on semiconductor surfaces at different ambient conditions. *Journal of the Optical Society of America B* **27**, 1077–1082.

Gekelman W, Van Zeeland M, Vincena S and Pribyl P (2003) Laboratory experiments on Alfvén waves caused by rapidly expanding plasmas and their relationship to space phenomena. *Journal of Geophysical Research: Space Physics* **108**, 8:1–8:10.

Hafeez S, Shaikh NM, Rashid B and Baig MA (2008) Plasma properties of laser-ablated strontium target. *Journal of Applied Physics* **103**, 083117–083124.

Harilal SS, Bindhu CV, Issac RC, Nampoori VPN and Vallabhan CPG (1997) Electron density and temperature measurements in a laser produced carbon plasma. *Journal of Applied Physics* **82**, 2140–2146.

Harilal SS, Bindhu CV, Nampoori VPN and Vallabhan CPG (1998*a*) Influence of ambient gas on the temperature and density of laser produced carbon plasma. *Applied Physics Letters* **72**, 167–169.

Harilal SS, Bindhu CV, Nampoori VPN and Vallabhana CPG (1998*b*) Temporal and Spatial behavior of electron density and temperature in a laser produced plasma from $YBa_2Cu_3O_7$. *Applied Spectroscopy* **52**, 449–455.

Harilal S, Tillack M, O'shay B, Bindhu C and Najmabadi F (2004) Confinement and dynamics of laser-produced plasma expanding across a transverse magnetic field. *Physical Review E* **69**, 026413.

Harilal SS, Sizyuk T, Hassanein A, Campos D, Hough P and Sizyuk V (2011) The effect of excitation wavelength on dynamics of laser-produced tin plasma. *Journal of Applied Physics* **109**, 063306.

Hayat A, Bashir S, Rafique MS, Akram M, Mahmood K, Iqbal S and Dawood A (2016) Spectroscopic and morphological study of laser ablated Titanium. *Optics and Spectroscopy* **121**, 1–9.

Huba J (2016) *NRL Plasma Formulary, (Naval Research Laboratory)*. Washington, DC: USA.

Iftikhar H, Bashir S, Dawood A, Akram M, Hayat A, Mahmood K, Zaheer A, Amin S and Murtaza F (2017) Magnetic field effect on laser-induced breakdown spectroscopy and surface modifications of germanium at various fluences. *Laser and Particle Beams* **35**, 159–169.

Iida Y (1990) Effects of atmosphere on laser vaporization and excitation processes of solid samples. *Spectrochim. Acta B* **45**, 1353–1367.

Joshi H, Kumar A, Singh R and Prahlad V (2010) Effect of a transverse magnetic field on the plume emission in laser-produced plasma: An atomic analysis. *Spectrochimica Acta B* **65**, 415–419.

Kaufman V and Martin WC (1990) Wavelength and energy level classification of magnesium spectra for all stages of ionization (Mg I through Mg XII). Gaithersburg: National Institute of Standards and Technology.

Kim TH, Nam SH, Park HS, Song JK and Park SM (2007) Effects of transverse magnetic field on a laser-produced Zn plasma plume and ZnO films grown by pulsed laser deposition. *Applied Surface Science* **253**, 8054–8058.

Li Y, Hu C, Zhang H, Jiang Z and Li Z (2009) Optical emission enhancement of laser-produced copper plasma under a steady magnetic field. *Applied Optics* **48**, B105–B110.

Neogi A and Thareja R (1999) Laser-produced carbon plasma expanding in vacuum, low pressure ambient gas and nonuniform magnetic field. *Physics of Plasmas* **6**, 365–371.

Ott E and Manheimer W (1977) Cross-field injection, propagation, and energy deposition of intense ion beams with application to tokamak plasma heating. *Nuclear Fusion* **17**, 1057.

Pandey PK and Thareja RK (2011) Plume dynamics and cluster formation in laser-ablated copper plasma in a magnetic field. *Journal of Applied Physics* **109**, 074901.

Pandey PK, Gupta SL and Thareja RK (2015) Study of pulse width and magnetic field effect on laser ablated copper plasma in air. *Physics of Plasmas* **22**, 073301.

Peyser T, Manka C, Ripin B and Ganguli G (1992) Electron–ion hybrid instability in laser-produced plasma expansions across magnetic fields. *Physics of Fluids B* **4**, 2448–2458.

Rai VN, Rai AK, Yueh F-Y and Singh JP (2003) Optical emission from laser-induced breakdown plasma of solid and liquid samples in the presence of a magnetic field. *Applied Optics* **42**, 2085–2093.

Raju MS, Singh R, Gopinath P and Kumar A (2014) Influence of magnetic field on laser-produced barium plasmas: spectral and dynamic behaviour of neutral and ionic species. *Journal of Applied Physics* **116**, 153301.

Reader J, Corliss CH, Wiese WL and Martin GA (1980) *Wavelengths and Transition Probabilities for Atoms and Atomic Ions*. Washington, DC: Center for Radiation Research,National Measurement Laboratory,National Bureau of Standards.

Rumsby P and Paul J (1974) Temperature and density of an expanding laser produced plasma. *Plasma Physics* **16**, 247.

Shaikh NM, Hafeez S and Baig MA (2007) Comparison of zinc and cadmium plasma parameters produced by laser-ablation. *Spectrochimica Acta B* **62**, 1311–1320.

Shen X, Lu Y, Gebre aT, Ling H and Han Y (2006) Optical emission in magnetically confined laser-induced breakdown spectroscopy. *Journal of Applied Physics* **100**, 053303.

Sherbini E, Mohmoud A, Aamer A and Saad AA (2012) Measurement of plasma parameters in laser-induced breakdown spectroscopy using Si-lines. *World Journal of Nano Science and Engineering* **2**, 206.

https://doi.org/10.1017/S0263034618000137 Published online by Cambridge University Press

Singh KS and Sharma AK (2016) Multi-structured temporal behavior of neutral copper transitions in laser-produced plasma in the presence of variable transverse static magnetic field. *Physics of Plasmas* **23**, 013304.

Singh KS and Sharma AK (2017) Time-integrated optical emission studies on laser-produced copper plasma in the presence of magnetic field in air ambient at atmospheric pressure. *Applied Physics A: Solids and Surfaces* **123**, 325.

Vladoiu I, Stafe M, Negutu C and Popescu IM (2008) Nano pulsed ablation rate of metals dependence on the laser fluence and wavelength in atmospheric air. *UPB Scientific Bulletin* **70**, 119–126.

Waheed S, Bashir S, Dawood A, Anjum S, Akram M, Hayat A, Amin S and Zaheer A (2017) Effect of magnetic field on laser induced breakdown spectroscopy of zirconium dioxide (ZrO_2) plasma. *Optik* **140**, 536–544.

Weyl GM (1989) Physics of laser-induced breakdown. In Dekker M (ed.), *Laser-Induced Plasmas and Applications*. New York: CRC Press, pp. 1–59,.

WikiPedia. https://en.wikipedia.org/wiki/Gilding_metal.

Ye C, Cheng GJ, Tao S and Wu B (2013) Magnetic field effects on laser drilling. *Journal of Manufacturing Science and Engineering-Transactions of ASME* **135**, 061020–1:5.

Yousaf D, Bashir S, Akram M, Kalsoom UI and Ali N (2013) Laser irradiation effects on the surface, structural and mechanical properties of Al–Cu alloy 2024. *Radiation Effects and Defects* **169**, 144–156.

https://doi.org/10.1017/S0263034618000137 Published online by Cambridge University Press